Catalysis Today 180 (2012) 139–147

Contents lists available at ScienceDirect

Catalysis Today

journal homepage: www.elsevier.com/locate/cattod

Redox and catalytic properties of Ce–Zr mixed oxide nanopowders for fuel cell applications

J. Kearney[1], J.C. Hernández-Reta, R.T. Baker*

EaStChem, School of Chemistry, University of St. Andrews, North Haugh, St. Andrews, Fife KY16 9ST, United Kingdom

ARTICLE INFO

Article history:
Received 15 December 2010
Received in revised form 19 April 2011
Accepted 25 May 2011
Available online 28 June 2011

It is a great pleasure to be able to contribute a few sheets to this issue in recognition of the career of Serafín Bernal, from whom I learned many important things.

Keywords:
Ce–Zr mixed oxide
Catalysis
Nanopowder
Methane
Redox
Solid oxide fuel cell

ABSTRACT

$Ce_xZr_{1-x}O_2$ mixed oxides nanopowders with $x = 0.10, 0.25, 0.50, 0.75$ and 0.90, and pure ceria, all prepared by a low temperature citrate complexion technique, were investigated using a range of temperature programmed (TP) techniques in order to evaluate their suitability for use as anode catalyst materials in solid oxide fuel cells operating on hydrocarbon fuels. In TP reduction experiments, reduction peak temperatures and peak areas were related to the activity and amount, respectively, of available catalyst oxygen. Mixed oxides with higher Ce contents ($x \geq 0.50$) were found to be reduced at significantly lower temperatures than samples with $x < 0.50$. The oxide with $x = 0.75$ supplied the largest amount of labile oxygen. TP reaction experiments performed in dry methane on two samples indicated that susceptibility of the oxides to carbon deposition was inversely related to availability of catalyst oxygen. Light-off experiments in a stoichiometric CH_4/O_2 mixture were performed to investigate the catalytic activity of the mixed oxide compositions for methane oxidation. Catalytic activity increased with cerium content to a maximum at $x = 0.75$ before decreasing at $x = 0.90$. All the mixed oxides were considerably more active for methane oxidation than pure CeO_2 prepared by the same citrate route.

1. Introduction

Mixed oxides of Ce and Zr have been investigated extensively for a range of applications, but are primarily used as automotive three-way catalysts (TWCs) [1–17]. TWCs are sited in the exhaust pipe of vehicles and convert CO, un-combusted hydrocarbons and NO_x from the engine into CO_2, H_2O and N_2 for release into the atmosphere. The incorporation of Zr into CeO_2 to give the $Ce_xZr_{1-x}O_2$ system has been clearly shown to increase both the thermal stability of the catalyst microstructure and the catalytic activity, especially for oxidation reactions [18,19]. These properties have resulted in the investigation of the Ce–Zr–O system for the catalytic combustion of hydrocarbons [14]. These properties also make these materials of interest for application in the fuel electrode (the anode) in SOFCs where hydrocarbon fuels are to be fed directly to the fuel cell.

As well as catalytic activity for the fuel reaction, the SOFC anode must possess good electronic conductivity. In SOFCs which operate on hydrogen fuels, an anode of Ni–YSZ is often used. Here the Ni acts as both catalyst and electronic conductor. However, in hydrocarbon fuels these anodes are deactivated and ultimately destroyed by deposition of carbon [20–22]. Oxides which can act as catalysts and are electronic conductors, or oxide catalysts coupled with metals other than Ni, are therefore of interest for direct utilisation of hydrocarbons in SOFCs. Cu has been shown to provide good electronic conductivity for the anode while being relatively inert with regard to carbon deposition reactions [23]. A large amount of research has been performed by Gorte and co-workers on the incorporation of CeO_2 – usually with Cu – as an active phase in the anodes of SOFCs, usually with yttria-stabilised zirconia (YSZ) electrolytes. These authors report impressive performance with hydrocarbon fuels [24–31]. Rather than being a problem, limited, preferential carbon deposition appeared to provide an improved electron conduction pathway after operation of the cell under n-butane, for example, so improving the overall conductivity of the Cu/CeO_2–YSZ anodes [24]. The performance of Ni–YSZ and Cu–CeO_2–YSZ anodes was compared by Costa-Nunes et al. when operating under H_2 and CO [27]. The Ni–YSZ anodes were found to be very effective when operating under H_2 but showed extremely poor performance with CO. However, a Cu–CeO_2 anode material deposited on the YSZ electrolyte showed comparable performance for both fuels. As a result, it was proposed that this anode would be able to operate directly with syngas fuels. The substitution of CeO_2 by $Ce_{0.6}Zr_{0.4}O_2$ in the Cu–CeO_2–YSZ system was shown by Ahn et al. [32] to significantly enhance the thermal stability of the material

* Corresponding author. Tel.: +44 1334 463899; fax: +44 1334 463808.
E-mail address: rtb5@st-andrews.ac.uk (R.T. Baker).
[1] Now at: CPI, Wilton Centre, Wilton, Redcar, Teesside TS10 4RF, United Kingdom.

0920-5861/$ – see front matter © 2011 Elsevier B.V. All rights reserved.
doi:10.1016/j.cattod.2011.05.018

when operated in humidified H_2. Larrondo et al. [18] investigated a range of $Ce_xZr_{1-x}O_2$ (x = 0.9, 0.7, 0.5) oxide powders for catalytic oxidation of H_2 and dry CH_4 and reported increased catalytic activity on incorporation of Zr into the CeO_2 lattice for all three oxide compositions. In a related study, these catalysts were found to improve performance over that of pure CeO_2 when incorporated into the anodes of a single chamber SOFC. Unlike in a conventional SOFC, in a single chamber cell both the anode and the cathode are exposed to a mixture of both the fuel and the oxidant, CH_4 and O_2 in this case [33].

The present contribution forms part of a larger, systematic study aimed at evaluating the suitability of Ce–Zr mixed oxide nanopowders for application in the anodes of SOFCs for use with hydrocarbon fuels directly. For the overall study it was necessary to prepare a compositional series of Ce–Zr oxide materials with consistent physical properties and suitable nanostructure. This was achieved by employing a low-temperature citrate complexation method. This yielded high-purity Ce–Zr mixed oxides whose structures resembled highly porous solid foams, or egg-shell structures, consisting of thin sheets of the mixed oxide material. These sheets were found to be comprised of well-defined nanocrystals with diameters of 8–10 nm, depending on chemical composition. The foam-like structure could be broken down and the nanoparticles released by grinding or milling. The resulting compositional series of nanopowders showed very consistent physical properties and so provided a good basis for the evaluation of Ce–Zr mixed oxides for use in SOFC anodes, the overall aim of the larger study. The thermochemical and crystallographic properties and the micro- and nanostructural characterisation of these materials have been reported elsewhere [34]. The findings of a detailed parallel electrochemical study of fuel cell electrodes incorporating these Ce–Zr oxide materials have been reported recently [35]. In this study, the electrochemical properties of the electrodes were studied using impedance spectroscopy, the spectra were fitted to a sophisticated fractal model and the fit parameters were used to compare electrode behaviour as a function of Ce–Zr oxide composition.

In the current contribution, the redox and catalytic properties of the above-mentioned compositional series of Ce–Zr oxide nanopowders were studied. Properties of interest for the intended final application of these materials in SOFC anodes were investigated using temperature-programmed (TP) techniques and other catalysis methods. The availability and quantity of catalyst oxygen species were studied by TP reduction. Catalyst deactivation through formation of carbon deposits under hydrocarbon fuels was addressed in experiments involving TP reaction followed by TP Oxidation. Finally, light-off curves for the oxidation of methane under stoichiometric conditions were recorded and the light-off temperatures were used to compare the catalyst samples in terms of their hydrocarbon activation ability. It was hoped that these results would provide insight into the potential of these materials for use in SOFC anodes. The findings of a parallel electrochemical study on fuel cell electrodes incorporating these Ce–Zr oxide materials showed interesting agreement with the results of the current catalytic study [35].

2. Materials and methods

2.1. Materials preparation

$Ce_{0.1}Zr_{0.9}O_2$ (CZ10), $Ce_{0.25}Zr_{0.75}O_2$ (CZ25), $Ce_{0.5}Zr_{0.5}O_2$ (CZ50), $Ce_{0.75}Zr_{0.25}O_2$ (CZ75) and $Ce_{0.9}Zr_{0.1}O_2$ (CZ90) oxide nanopowders, and pure CeO_2, were synthesised from nitrate precursors using a citrate complexation method established in the group and described previously [36–38]. Briefly, zirconium dinitrate oxide (99.9%, Alfa Aesar) and cerium nitrate hexahydrate (99.5%, Alfa Aesar) were weighed in the ratio appropriate for the preparation of 0.1 mol of the relevant oxide before being dissolved separately in 50 ml of deionised (d.i.) water under stirring. These two cation solutions were combined and left to mix under stirring. An amount of anhydrous citric acid (99.5%, Alfa Aesar) appropriate to give a molar ratio of citric acid (CA):total oxide (TO) of 2:1 was dissolved in d.i. water and added to the cation solution. This solution of citric acid and the two nitrates (only one to make ceria) was allowed to homogenise under stirring before the temperature was increased at a rate of 5 °C min^{-1} to 80 °C for 30 min. This step caused the elimination of excess water and the formation of a transparent gel which became increasingly viscous over time. The gel was transferred to a muffle furnace and was heated to 250 °C for 1 h at a heating rate of 2 °C min^{-1}. This led to the evolution of the remaining water and of gaseous nitrogen oxides. The resulting foam-like powder was calcined by heating to 500 °C for 1 h at a rate of 2 °C min^{-1}. These calcined powders were ground using a pestle and mortar to give fine powders for study of their redox and catalytic properties in temperature programmed reduction and light-off experiments. Specific Surface Areas (SSAs) of the samples were obtained by the BET method using N_2 adsorption and desorption in a Micrometrics instrument.

Details of the thermochemical and crystallographic properties and of the micro- and nanostructure of these materials, including high resolution XRD patterns of the nanopowder samples used in the current study can be found elsewhere [34]. The current contribution addresses the redox properties and catalytic activity of these materials. XRD patterns of a number of samples after use in certain of these experiments were recorded on a STOE Stadip instrument using Cu Kα radiation with a step size of 0.5° and step time of 15 s. These patterns are available as Supplementary Data.

2.2. Temperature programmed experiments

The system used for the temperature programmed (TP) experiments was based on that used by Baker and Metcalfe [39] and was designed and built in house. Gases and gas mixtures were supplied to the system from cylinders (B.O.C. Ltd.). An inert gas, Ar, and three dilute treatment gases, 5% H_2/Ar, 5% CH_4/Ar and 5% O_2/Ar were used and these were passed through water traps and oxygen traps (except the O_2/Ar) before entering the TP system. In addition, a calibration gas could be connected to the system. The treatment gas to be used was selected using a four-way valve. Two mass flow controllers (MFCs, UNIT) were used to set up two equivalent, precisely controlled, continuous parallel flows of the inert and of the selected treatment gas. One of these gases passed to vent while the other passed to the TP microreactor. Because both flows were continuous, their routes could be switched over without the risk of introducing contaminant gases, such as air, into the reactor system. The exit gas from the microreactor flowed through a manifold of differentially-pumped control valves which split off a small fraction for analysis in the quadrupole mass spectrometer (QMS), the remainder going to vent. The TP microreactor could be bypassed – to protect the sample, for example – and the system was equipped with a water injection port which was used to calibrate the QMS response. The calibration was obtained by injection of 1 μl aliquots of d.i. water each day. Downstream of the liquid injection port all tubing was glass-lined and was trace heated to prevent condensation of water or other species in the apparatus. The tubular quartz micro-reactors were built in-house and contained a central quartz frit on which the sample was located. Accurate sample heating was achieved using a small resistive furnace controlled by a dedicated temperature controller. Typical sample mass was 50 mg. This ensured that the quartz frit was completely covered in sample without there being excessive depth of catalyst bed which may have resulted in significant re-adsorption of desorbing species. The QMS system was

able to log up to 16 separate mass to charge ratios (m/q) in real time and software was used to convert these data and the temperature signal from the microreactor into TP spectra. The main ratios used were m/q = 2, 15, 18, 28, 32 and 44 which corresponded to H_2, methane (i.e. CH_3), water, CO (and N_2), O_2 and CO_2. Traces for C, N and O, which resulted from fragmentation of primary species in the QMS, were employed to clarify ambiguities in the traces of the main species. Gas flow rates of 50 ml min^{-1} and TP heating rates of 5 °C min^{-1} were used throughout. Desorption of species from the surface of a catalyst could be followed as a function of temperature in TP desorption (TPD, in inert, *e.g.* Ar). The system also allowed TP Reduction (TPR, following H_2O production in 5% H_2/Ar), reaction (TPRx, following various products and reactants in *e.g.* 5% CH_4/Ar) and Oxidation (TPO, O_2 consumption and oxygenate production in 5% O_2/Ar) experiments to be performed.

2.3. Light-off experiments

The light-off experiments were performed using the apparatus described above. This was modified slightly to allow dilute methane (5% CH_4 in Ar) and oxygen (5% O_2 in Ar) gases to be mixed so as to give a stoichiometric molar ratio of O_2:CH_4 = 2. This gas mixture was supplied to the microreactor at a flow rate of 50 ml min^{-1} (at standard pressure). Samples (50 mg) were pre-reduced *in situ* by heating to 500 °C in a flow of 5% H_2/Ar (50 ml min^{-1}) at 5 °C min^{-1}. Once the sample had cooled to ambient, the reactor was flushed with Ar, the flow of the stoichiometric CH_4/O_2 mixture was established and the sample was heated at 5 °C min^{-1} to the maximum temperature, 900 °C. A sample of the outlet gas was passed to the QMS which allowed the consumption of the reactants (CH_4 and O_2) and the generation of the products (CO_2, H_2O for total oxidation and CO and H_2 for partial oxidation) to be monitored in real time. The more active the catalyst sample under test the lower the temperature at which reaction was observed to start, or 'light off', giving rise to an initial exponential increase in partial pressures of the products and a matching decease in the partial pressures of the reactants. The light-off temperature was defined here as the temperature at which 10% of maximum conversion was attained [40]. This provides a convenient way to compare the activity of a number of catalyst samples. Usually, light-off experiments are performed under steady state conditions at a number of isothermal points. In the present contribution the product and reactant partial pressures were recorded continuously as temperature was slowly and linearly increased (at 5 °C min^{-1}). This method is quicker and more convenient than the former method and, if some care is taken in their interpretation, gives useful and meaningful results.

3. Results and discussion

3.1. Temperature programmed reduction

The traces of water evolution (m/q = 18) during the TPR experiments for all of the as-prepared CZ samples and for ceria are presented in Fig. 1. The areas under the peaks are directly comparable between samples and relate to the number of moles of water released. The peaks can be divided into two groups. Firstly, those that occur at around 100 °C would appear to be caused by desorption from the samples of physisorbed water molecules. The second set of peaks occurs at much higher temperature. These peaks show variation in peak area with composition and also a much more marked variation in peak position on the temperature scale. It is likely that these peaks are the result of reduction of the catalysts by H_2 rather than of desorption of water pre-existing on the catalyst surface. To confirm the assignments of these two sets of peaks, fresh samples of each composition were subjected first to a TPD

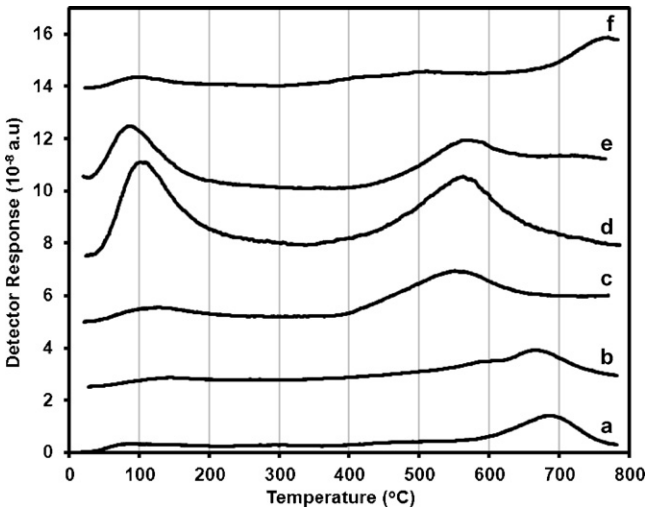

Fig. 1. Water traces from the TPR experiments for (a) CZ10, (b) CZ25, (c) CZ50, (d) CZ75, (e) CZ90 and (f) CeO_2.

experiment to 800 °C in flowing Ar, and then, after cooling to ambient, to the TPR experiment as normal. During the TPD experiment any physisorbed species would be expected to desorb whereas no, or little, reduction would be expected in the Ar atmosphere used. The water traces recorded during these TPR runs are presented in Fig. 2. It is possible to verify that the high temperature peaks remain largely as in Fig. 1 but that the low temperature water peaks are no longer present in the spectra. Further evidence for these assignments is presented in Fig. 3. Fig. 3(a) shows the H_2 and water traces during a standard TPR (without prior TPD). It is clear that consumption of H_2 was coincident with the high temperature water production peak but not with the low temperature water peaks, which have been attributed to desorption of physisorbed water. In addition, the water traces from the TPD, TPR and TPR after TPD (named TPD/R) are compared in Fig. 3(b). Again, the high temperature peaks in the TPRs with and without prior TPD are very similar, and not present in the TPD itself, while the low temperature peaks are present in the 'straight' TPR and in the TPD but not in the TPR with prior TPD. Therefore, the high temperature peaks can indeed be attributed to the reduction of the samples while those at around 100 °C were caused by desorption of pre-

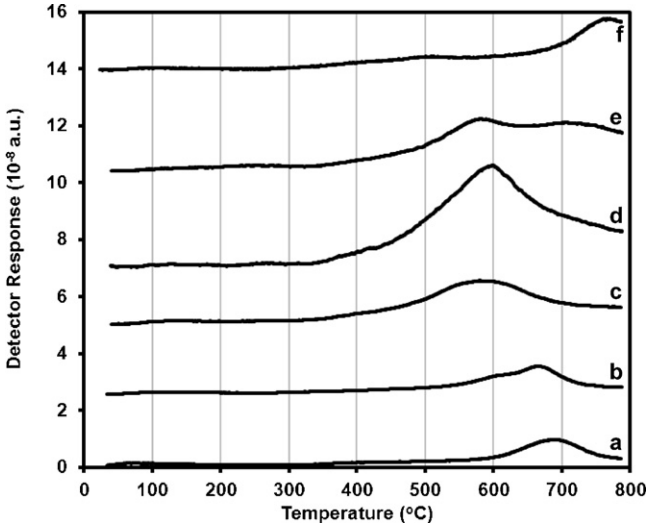

Fig. 2. Water traces from the TPR experiments after prior TPD (TPD/R in text) for (a) CZ10, (b) CZ25, (c) CZ50, (d) CZ75, (e) CZ90 and (f) CeO_2.

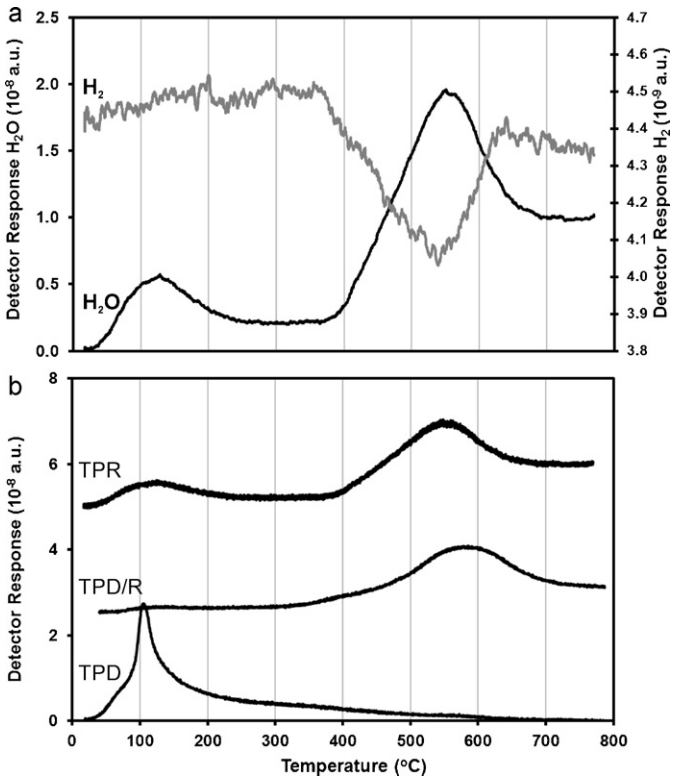

Fig. 3. Reduction behaviour of CZ50. (a) H_2 and water traces during a straight TPR experiment (H_2 trace shifted down *y*-axis for clarity) and (b) comparison of water traces from the TPD, TPR and TPD/R experiments.

existing physisorbed water. Although the samples were stored in a desiccator, it is clear that they took up water during handling in air.

To investigate the structure of the materials after these reduction experiments, XRD patterns of samples after use in the TPR experiments are presented in the Supplementary Data as Fig. S1. These are consistent with single phase Ce–Zr mixed oxides.

In oxidation catalysts, both the reactivity (or availability) of their oxygen as well as the amount of available oxygen are important factors. The high temperature peaks in the TPRs in Figs. 1 and 2 provide information on both. Firstly, the peak position is related to the reactivity of catalyst oxygen; the lower the peak temperature the more reactive the oxygen. Secondly, the area under the peaks can be quantified and calibrated to obtain the number of moles of water produced per unit mass of catalyst.

The positions of the main reduction peaks from Fig. 1 (TPRs) and Fig. 2 (TPD/Rs) are plotted for all compositions in Fig. 4. The peak

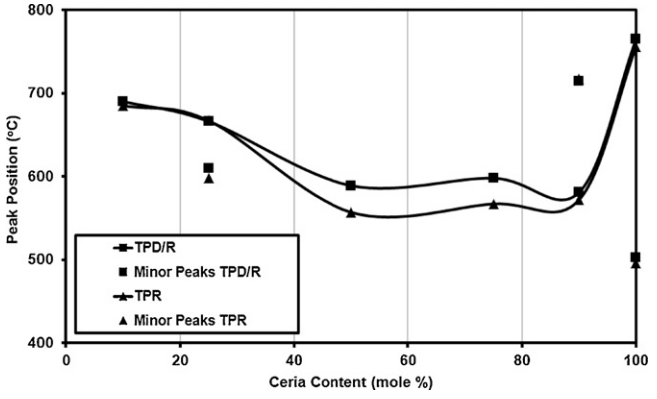

Fig. 4. Reduction peak positions (in °C) as a function of sample composition from the TPR and TPD/R experiments.

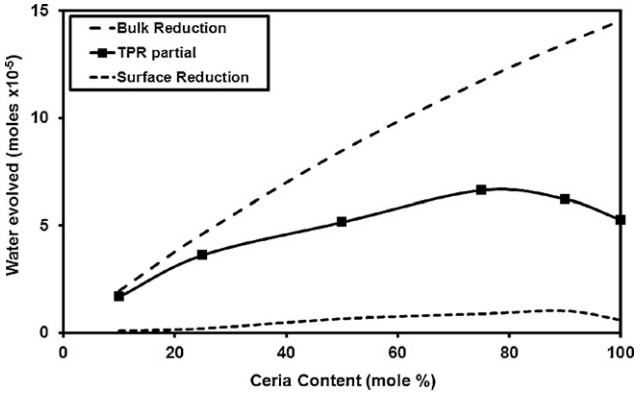

Fig. 5. Moles of water evolved as a result of sample reduction in the TPR (see text) as a function of sample composition. The theoretical maximum bulk and surface values are plotted for comparison.

positions for the latter tend to be slightly higher than for the TPRs without prior TPD. This can be explained as a slight coarsening of the nanostructure of the oxides during the additional temperature ramp to 800 °C in the TPD. However, the overall trend in both sets of data is essentially the same. Samples with the higher Ce contents – CZ50, CZ75 and CZ90 – gave rise to the lower temperature peaks – 557, 567 and 572 °C in the TPRs and 589, 598 and 581 °C in the TPD/Rs, respectively, whereas for CZ10 and CZ25 the main peak temperatures were about 100 °C higher and the pure ceria exhibited by far the highest main reduction peak, at around 770 °C. Therefore, the former group of samples seems to be the more promising in terms of oxygen activity. The peak positions determined here show very good agreement with those of fresh samples of similar compositions studied as part of a very detailed investigation of the Ce–Zr mixed oxide system by Vidal and co-workers [15,41].

Turning to the quantity of available oxygen, the amount of water evolved during the reduction experiments can be calculated by integrating the water trace in the TPR runs, subtracting the background and applying the water calibration of the QMS. In Fig. 5 the water production calculated by integrating the straight TPR trace from 300 °C up to the maximum temperature is plotted as a function of sample composition. This avoids including the low temperature water desorption peaks. This dataset has the advantage that a prior TPD run is not necessary, and so any thermally induced changes in the samples are avoided. However, if some reduction of the sample does occur at low temperatures (below 300 °C here), this would not be registered by this method but would be included in the TPD/R data. However, examination of the latter plots indicated that there were only very small or no reduction features in this temperature range. For comparison, the water which would be produced from complete reduction of the sample bulk is plotted in Fig. 5. This was calculated by assuming that all the Ce in the oxide samples was present as Ce^{4+} initially and that this would all be reduced to Ce^{3+} during the TPR, if complete reduction had taken place. In addition, the water which would be produced by complete reduction of the surface layer only of each sample is also given. This was calculated on the basis of the SSAs of each composition, their Ce content, and the expectation that a 25% reduction would occur, as for the bulk calculation. The method assumes (1 0 0) surface planes and follows the method of Zhao and Gorte [42]. It is clear from Fig. 5 that much more than just the surface oxygen is removed in the TPRs and that the degree of reduction represents a significant fraction of complete bulk reduction for each composition. The curve starts close to the theoretical bulk maximum for low Ce contents and rises to CZ75 before decreasing through CZ90 and, finally, pure ceria. Therefore, in terms of moles of available oxygen per gram of catalyst, CZ75 is best, followed by CZ90, ceria and CZ50. The water

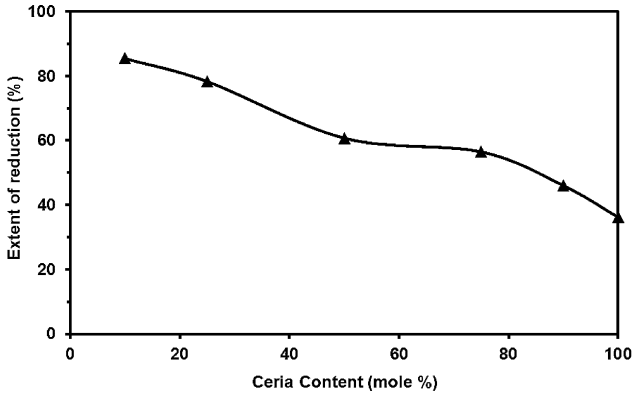

Fig. 6. Extent of sample reduction in the TPR experiments as a function of sample composition.

production data are re-plotted as a percentage of maximum calculated bulk oxidation in Fig. 6. There is a smooth decrease from 83% reduction for CZ10 to 40% for pure ceria. This trend is also similar to those reported by Vidal et al. [15,41].

Fig. 7(a) presents the significant variation in SSA with sample composition, and in Fig. 7(b) the amounts of water produced in the TPR experiments are normalised with respect to SSA. An approximately monotonic increase is seen with increasing Ce content in Fig. 7(b), favouring the pure ceria material. It is clear that low SSA had a negative effect on the CZ10, CZ25 and pure ceria materials.

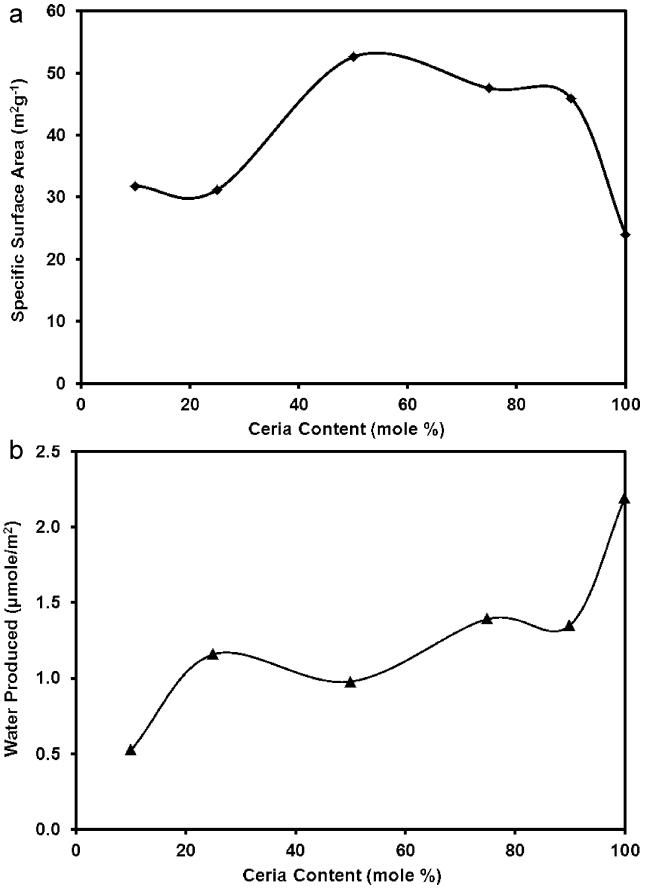

Fig. 7. (a) Specific surface area (SSA) of samples as a function of composition and (b) water production in TPR experiments normalised to sample SSA.

3.2. Temperature programmed reaction and oxidation

In order to study the extent of carbon deposition, TPRx experiments in dry, dilute methane were performed on the CZ50 and CZ90 samples to a maximum temperature of 900 °C. After cooling to ambient temperature, the samples were subjected to a TPO experiment in dilute oxygen to 800 °C. The resulting TPRx and TPO spectra are given in Fig. 8. In the TPRx spectra, the CH_4 trace has been moved well down the *y*-axis in order to compare the changes in this trace with those of the products. Since CH_4 is present at a much higher partial pressure than the products, a lower sensitivity scale must be used and the CH_4 trace thus appears much noisier than the others. Nevertheless, a large trough indicates consumption of CH_4 at high temperatures for both samples. This gives rise to significant CO evolution and this is accompanied by evolution of H_2, as seen, in an expanded trace, for the CZ90 sample. No H_2 appears to accompany CO evolution for the CZ50 sample, however, it perhaps being adsorbed onto the sample surface (see comments on light-off results in the next section). Since the samples were used as prepared in the TPRx experiments, there was some desorption of water and, to a lesser extent, CO_2 at about 100 °C. Finally, both TPRx plots indicate limited formation of products of complete oxidation – water and CO_2 – between about 300 °C and 900 °C with peaks at about 620 °C for CZ50 and about 800 °C for CZ90. It is clear that some oxygen from the catalyst reacted at these temperatures in the complete oxidation of CH_4. As this oxygen became depleted, products of partial oxidation, CO and H_2, dominated at higher temperatures, peaking at around 850 °C. In CZ90 the consumption of CH_4 was coincident with the release of CO, as would be expected. However, for CZ50 a small CH_4 consumption feature was coincident with CO release but the maximum in CH_4 consumption occurred after the maximum in CO production. This suggests that the CH_4 was being consumed to form surface carbon species.

Turning to the TPO results in Fig. 8(c) and (d), the main O_2 consumption feature coincides in both cases with formation of CO_2. This is consistent with the oxidation of surface carbon species (the C peak, and the CO peak in large part, occur as fragmentation products of CO_2 once it had entered the QMS). Two types of carbon species are indicated in each sample. The more reactive form gave rise to CO_2 peaks at lower temperature – 300 °C for CZ50 and 280 °C for CZ90 – and a much less reactive, probably polymeric form, resulted in CO_2 peaks at 590 °C and at 690 °C for CZ50 and CZ90, respectively. The O_2 trace was moved well down the *y*-axis and is very noisy because of the sensitivity setting used. However, in the TPO for CZ50 there is clearly a trough indicating consumption of O_2 before the evolution of the CO_2. This is likely to be caused by the re-oxidation of the catalyst itself. The amount of carbon deposition in these two catalysts was quantified from the areas of the CO_2 peaks and showed a ratio for CZ50 to CZ90 of 2.2:1. This is consistent with the larger amount of available oxygen for the CZ90 than the CZ50, as determined by the TPR experiments and presented in Figs. 5 and 6, which would tend to prevent carbon deposition in the initial TPRx run. An alternative explanation for consumption of O_2 and simultaneous release of CO_2 would be the conversion of cerium(III) carbonate, formed during the TPRx run, into CeO_2. The XRD pattern of a ceria sample recorded immediately after use in a TPRx run is given in the Supplementary Data. There was no evidence of cerium carbonates.

3.3. Light-off experiments

Light-off experiments were performed on all five CZ samples and on the pure ceria sample prepared using the same citrate complexation method. Samples were activated *in situ* by reducing in dilute H_2 to 500 °C. A blank light-off experiment was run using an empty

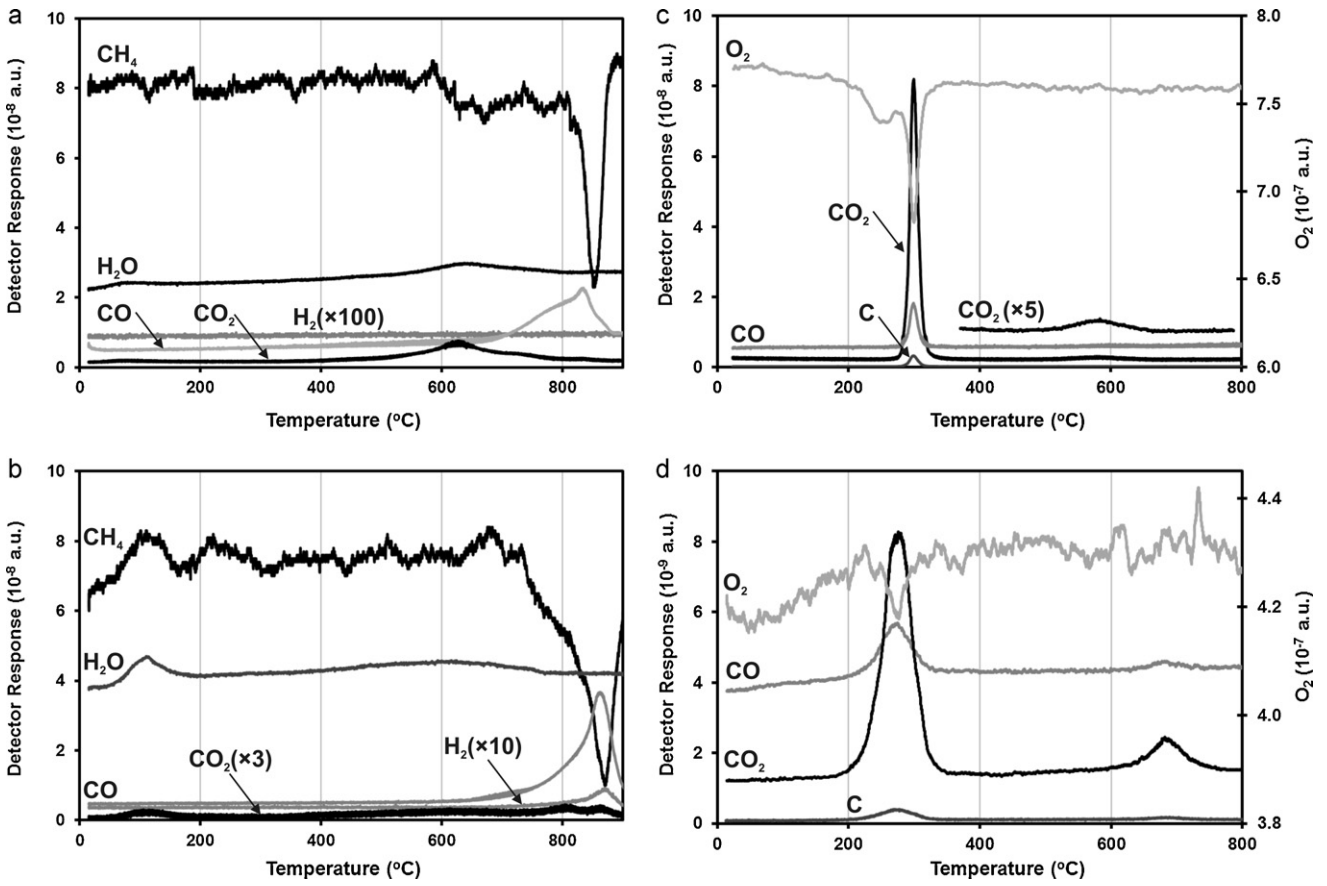

Fig. 8. Outlet gas compositions for TPRx experiments on (a) CZ50, (b) CZ90 and for TPO experiments on, (c) CZ50 and (d) CZ90. (O_2 traces are shifted down *y*-axis in TPOs for clarity.)

micro-reactor (data not shown). At around 700 °C there were large increases in the levels of H_2, H_2O, CO and CO_2 with corresponding decreases in CH_4 and O_2 indicating the onset of gas-phase reaction. Traces reached plateaux at temperatures from 800 °C.

In Fig. 9 the traces for the two reactants and four main products – H_2, H_2O, CO and CO_2 – in the light-off experiments are collected together for the five CZ samples and ceria. The reactant levels for all catalyst samples remained at their initial values up to 400 °C. The most active of the catalysts then began to catalyse the reaction between the CH_4 and O_2. As would be expected, the traces of both reactants showed the same order of activity for the catalysts tested. The CZ75 was noticeably more active than the other compositions. CZ25 and CZ50 together were the next active, it being difficult to tell their corresponding traces apart. CZ90 was the next active material and CZ10 the least active of the mixed oxides. Once the CZ10 had started to catalyse the reaction, however, the rate of increase of reaction rate with temperature was higher than for the CZ90, which it overtook, in terms of conversion, at around 550 °C. The CeO_2 prepared by the same method as the other materials was much less active than the mixed oxides. The O_2 traces fell to a constant level close to zero between 700 and 810 °C, depending on the material. The CH_4 traces displayed a similar initial pattern before a second sharp dip between 815 °C and 880 °C, again depending on the material. The CO_2 and water traces in Fig. 9(c) and (d), respectively, are, to an extent, the mirror images of the reactant traces. That is, they began to increase at some point above 400 °C (the exact temperature depending on the material) and they displayed the same order of activity, CZ75 > CZ25 ~ CZ50 > CZ10 > CZ90 > CeO_2. As was seen in the CH_4 trace, both the water and CO_2 traces displayed a dip for all catalyst compositions at some point between 815 °C and 890 °C. In the case of CO_2, despite the dip, the level was still well above the initial background level for all materials. These changes indicate that the water was being consumed in the steam reforming of methane at high temperature (above 800 °C) to generate CO and H_2. The CO and H_2 traces in Fig. 9(e) and (f), respectively reveal the temperature at which the steam reforming of methane occurred. CO was also recorded at lower temperatures (*e.g.* from 450 °C for CZ75), though there was no corresponding H_2 signal so it is likely that this CO feature was an artefact resulting from the breakdown of CO_2 in the QMS. CO and H_2 were released together, however, in a very sharp high temperature (815–890 °C) step feature as a result of the steam reforming of CH_4. The temperature at which this occurred varied between the samples.

Returning to the onset of the complete oxidation reaction, the light-off temperature is defined in this work as the temperature at which 10% of the maximum conversion of the reactants (or 10% of maximum generation of products) occurred. In Fig. 10 light-off temperatures for the two reactants and the two products of complete oxidation are plotted in order to compare the activities of the different catalysts. There is some variation in absolute temperature value, according to which chemical species is followed. However, the trends are all the same. Catalytic activity increased with increasing % Ce up to CZ75 before tailing off sharply. The CeO_2 had the highest light-off temperature by almost 80 °C. Hence, the mixed oxide nanopowders all appear to be far more active than the pure CeO_2 for catalysing the oxidation of methane. Also, importantly, the results are in agreement with the outcomes of the TPR and TPD/R experiments in that CZ75 appears to be the most active catalyst since it showed the lowest light-off temperature in all cases. However, CZ90 was considerably less active than CZ75 in the light-off experiments despite displaying nearly as good oxygen-donating

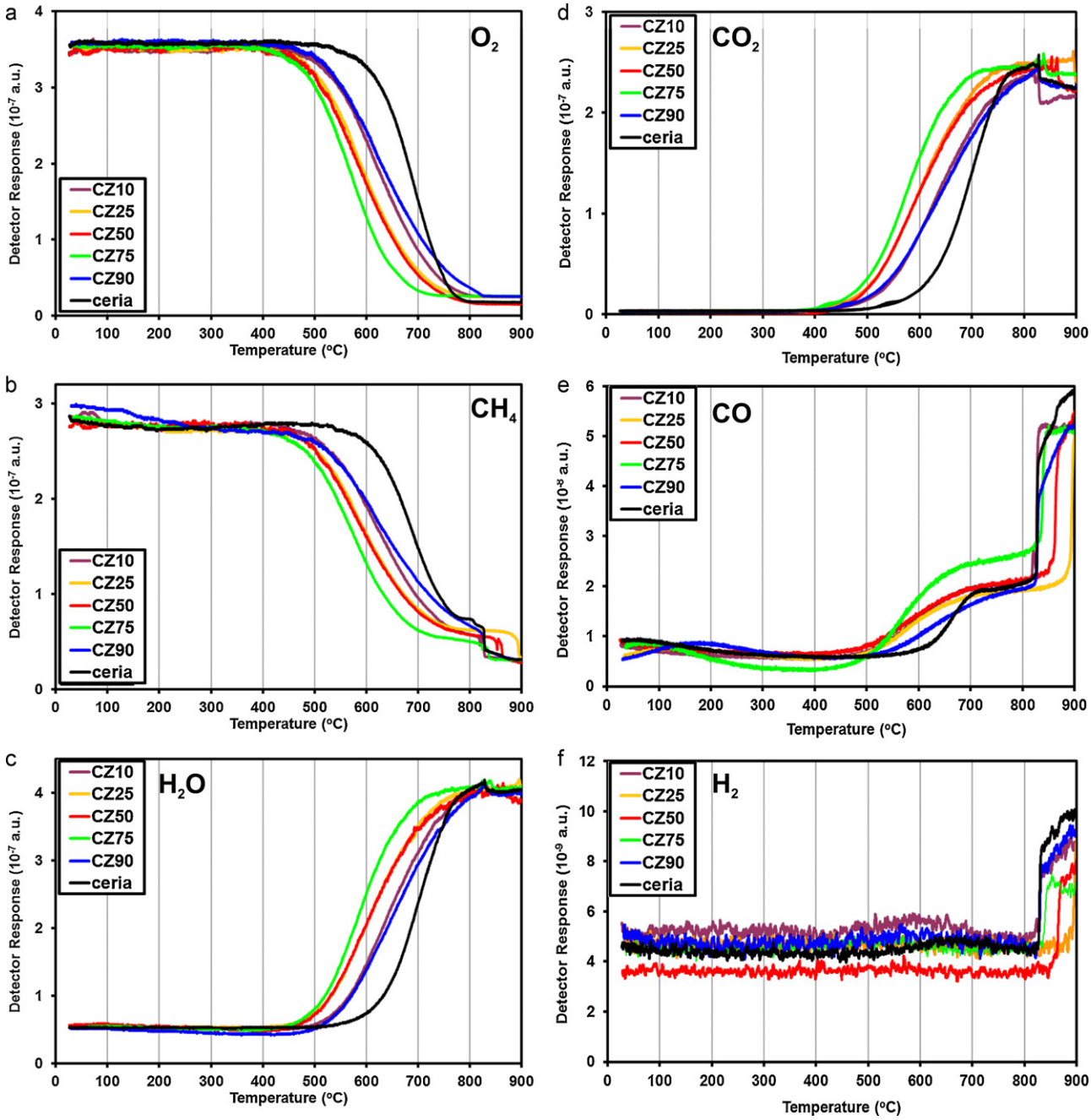

Fig. 9. Light-off curves for all CZ samples and for ceria showing (a) O_2 consumption, (b) CH_4 consumption, (c) water evolution, (d) CO_2 evolution, (e) CO evolution and (f) H_2 evolution.

properties. This suggests that CZ75 may be better at activating the methane molecule than CZ90, and that it is not simply a question of oxygen supply.

The differences in the light-off temperatures obtained by following the four different chemical species are interesting and can be explained because the experiment was performed under transient conditions rather than, as is more typical, under steady state. The CH_4 consumption and CO_2 production traces showed a good correlation as did those for O_2 consumption and H_2O production. However, the light-off temperatures for the latter were consistently around 20 °C higher than those observed for the carbon species, for all oxide samples, as is seen in Fig. 10. The difference between the temperatures at which CH_4 and O_2 partial pressures decrease can be explained by a mechanism in which the CH_4 reacts initially with oxygen species from the catalyst to form CO_2. The lost oxygen would then be replenished i.e. the catalyst re-oxidised – at slightly higher temperature by O_2 from the gas phase, so giving rise to the O_2 consumption feature, but at a slightly higher temperature than for CH_4 consumption. This explanation is consistent with the characterisation of Ce–Zr oxides as oxygen buffers in catalysis. It then appears that the hydrogen released in the breakdown of CH_4 was retained on the catalyst surface, most probably as stable OH^- species. This would account for the slightly higher temperature at which H_2O is produced, compared to that of CH_4 consumption. If these species were relatively stable then this would explain the temperature lag between the consumption of CH_4 and the combination of these surface hydroxide groups to release H_2O. Zhao and Gorte investigated the oxidation of four hydrocarbons, including methane and n-butane, over CeO_2 and Sm-doped CeO_2 and reported some interesting conclusions [42]. They found that

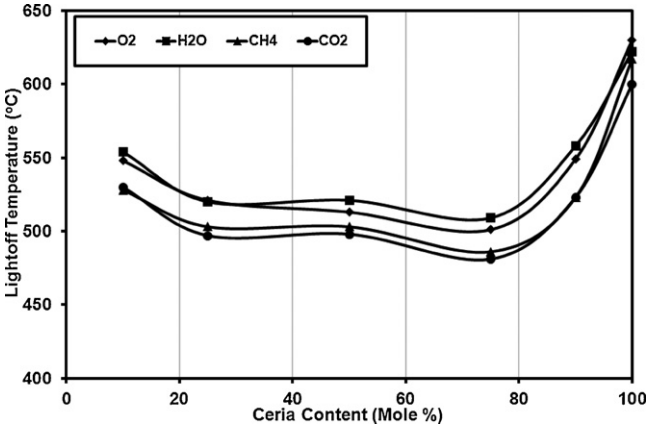

Fig. 10. Light-off temperatures as a function of sample composition as determined from the traces for consumption of O_2 and of CH_4 and for evolution of water and of CO_2.

exchange of oxygen between the bulk and the surface of their ceria began at about 377 °C and that the availability of bulk oxygen above this temperature had an effect on the mechanism of hydrocarbon oxidation. For butane, below about 377 °C, a reaction regime of half order in O_2 suggested reaction of atomic surface O with the hydrocarbon in the rate determining step. At higher temperatures, the reaction became zero order in O_2, indicating reaction of lattice, or bulk, oxygen with the hydrocarbon followed by its replacement from the gas phase, as discussed here in relation to the light-off curves. Activation of CH_4 was thought to be more difficult than that of butane, because CH_4 lacks the more reactive $-CH_2-$ groups. The authors proposed that, because of this, only the high temperature, zero-order reaction took place with CH_4. Furthermore, because of the difficulty of activating methane, the surface and chemical properties of the catalyst play an important role and activity for H_2 activation may not always be a good guide to activity for methane activation. This is relevant to the current work in which CZ75 and CZ90 had similar redox properties and SSAs and yet CZ75 was considerably more active in the light-off experiments.

4. Conclusions

The redox behaviour and catalytic activity of five different Ce–Zr mixed oxides and CeO_2 were investigated using a series of temperature programmed experiments. Samples containing at least 50 mol% ceria were reduced at similar temperatures (581–598 °C in the TPD/Rs) and samples with lower ceria content were reduced at significantly higher temperatures (666–690 °C in the TPD/Rs). The thermal cycling associated with the TPD experiments led to a small increase in the reduction temperature in the subsequent TPR for most samples. To avoid this effect, reduction was quantified using the high temperature region of the TPR plot. CZ75 produced the greatest amount of oxygen (to form water) per unit mass in the TPR experiments. The highest percentage of theoretical water yield was observed for the CZ10 sample, in agreement with the literature, although this sample also produced the least water in absolute terms.

Light-off experiments allowed comparison of the catalytic activity of the samples for methane oxidation. The most active sample was found to be CZ75. The CZ25 and CZ50 were less active, and the CZ10 and CZ90 the least active, of the mixed oxides. However, even the least active mixed oxides had a light-off temperature 80 °C lower than that of pure ceria. Further work on the activity of these materials for oxidation of different hydrocarbon fuels under steady-state conditions would be useful to elucidate the effects of different reaction mechanisms and the influence of catalyst SSA.

Overall, the results indicated that the CZ75 mixed oxide is the most promising catalyst for methane oxidation. It showed one of the lowest reduction temperatures, the largest absolute oxygen availability as well as the lowest light-off temperature for methane oxidation. It is interesting to note that, in a recently reported electrochemical study, electrodes containing the CZ materials studied here demonstrated that the CZ75 electrode had the lowest polarisation resistance in impedance spectroscopy measurements under H_2- and CH_4-containing atmospheres [35]. This material is therefore of interest for application in anodes for SOFCs operating on hydrocarbon fuels.

Acknowledgements

This work was funded by the Engineering and Physical Sciences Research Council of the U.K. and was performed within the Supergen Fuel Cell Consortium (Phase one). We are grateful for a Mexican Government Conacyt Scholarship for JCHR.

Appendix A. Supplementary data

Supplementary data associated with this article can be found, in the online version, at doi:10.1016/j.cattod.2011.05.018.

References

[1] H. Vidal, S. Bernal, J. Kašpar, M. Pijolat, V. Perrichon, G. Blanco, J.M. Pintado, R.T. Baker, G. Colon, F. Fally, Catal. Today 54 (1999) 93.
[2] R. Di Monte, J. Kašpar, Catal. Today 100 (2005) 27.
[3] J. Kašpar, P. Fornasiero, G. Balducci, R. Di Monte, N. Hickey, V. Sergo, Inorg. Chim. Acta 349 (2003) 217.
[4] Y. Guo, G. Lu, Z. Zhang, S. Zhang, Y. Qi, Y. Liu, Catal. Today 126 (2007) 296.
[5] G. Colon, M. Pijolat, F. Valdivieso, H. Vidal, J. Kašpar, E. Finocchio, M. Daturi, C. Binet, J.C. Lavalley, R.T. Baker, S. Bernal, J. Chem. Soc., Faraday Trans. 94 (1998) 3717.
[6] S. Bernal, G. Blanco, J.J. Calvino, J.M. Gatica, J.A. Perez-Omil, J.M. Pintado, Top. Catal. 28 (2004) 31.
[7] R. Di Monte, J. Kašpar, Top. Catal. 28 (2004) 47.
[8] S. Bernal, G. Blanco, M.A. Cauqui, M.P. Corchado, C. Larese, Catal. Today 53 (1999) 607.
[9] M. Zhao, M. Shen, J. Wang, J. Catal. 248 (2007) 258.
[10] T. Masui, K. Minami, K. Koyabu, N. Imanaka, Catal. Today 117 (2006) 187.
[11] J. Kašpar, P. Fornasiero, J. Solid State Chem. 171 (2003) 19.
[12] J.R. González-Velasco, M.A. Gutiérrez-Ortiz, J.-L. Marc, J.A. Botas, M.P. González-Marcos, G. Blanchard, Appl. Catal. B 22 (1999) 167.
[13] V.R. Mastelaro, V. Briois, D.P.F. de Souza, C.L. Silva, J. Eur. Ceram. Soc. 23 (2003) 273.
[14] D. Terribile, A. Trovarelli, C. de Leitenburg, A. Primavera, G. Dolcetti, Catal. Today 47 (1999) 133.
[15] H. Vidal, J. Kašpar, M. Pijolat, G. Colon, S. Bernal, A. Cordon, V. Perrichon, F. Fally, Appl. Catal. B 27 (2000) 49.
[16] F. Zamar, A. Trovarelli, C. de Leitenburg, G. Dolcetti, Chem. Commun. (1995) 965.
[17] A.B. Hungria, N.D. Browning, R.P. Erni, M. Fernández-Garcia, J.C. Conesa, J.A. Pérez-Omil, A. Martinez-Arias, J. Catal. 235 (2005) 251.
[18] S. Larrondo, M.A. Vidal, B. Irigoyen, A.F. Craievich, D.G. Lamas, I.O. Fabregas, G.E. Lascalea, N.E.W. de Reca, N. Amadeo, Catal. Today 107–108 (2005) 53.
[19] L.F. Liotta, G. Di Carlo, G. Pantaleo, G. Deganello, Appl. Catal. B 70 (2007) 314.
[20] J. Maček, B. Novosel, M. Marinšek, J. Eur. Ceram. Soc. 27 (2007) 487.
[21] M. Mogensen, S. Skaarup, Solid State Ionics 86–88 (1996) 1151.
[22] R.T. Baker, I.S. Metcalfe, Ind. Eng. Chem. Res. 34 (1995) 1558.
[23] A. Fuerte, R.X. Valenzuela, L. Daza, J. Power Sources 169 (2007) 47.
[24] S. Park, J.M. Vohs, R.J. Gorte, Nature 404 (2000) 265.
[25] H. He, J.M. Vohs, R.J. Gorte, J. Electrochem. Soc. 150 (2003) A1470.
[26] S. Jung, C. Lu, H. He, K. Ahn, R.J. Gorte, J.M. Vohs, J. Power Sources 154 (2006) 42.
[27] O. Costa-Nunes, R.J. Gorte, J.M. Vohs, J. Power Sources 141 (2005) 241.
[28] M.D. Gross, J.M. Vohs, R.J. Gorte, J. Electrochem. Soc. 154 (2007) B694.
[29] C. Lu, W.L. Worrell, J.M. Vohs, R.J. Gorte, J. Electrochem. Soc. 150 (2003) A1357.
[30] C. Lu, W.L. Worrell, R.J. Gorte, J.M. Vohs, J. Electrochem. Soc. 150 (2003) A354.
[31] S.-I. Lee, J.M. Vohs, R.J. Gorte, J. Electrochem. Soc. 151 (9) (2004) A1319.
[32] K. Ahn, H. He, J.M. Vohs, R.J. Gorte, Electrochem. Solid State Lett. 8 (8) (2005) A414.

[33] D.G. Lamas, M.D. Cabezas, I.O. Fábregas, N.E. Walsöe de Reca, G.E. Lascalea, A. Kodjaian, M.A. Vidal, N.E. Amadeo, S.A. Larrondo, Electrochem. Soc. Trans. 7 (2007) 941.
[34] R.O. Fuentes, R.T. Baker, J. Phys. Chem. C 113 (2009) 914.
[35] S. Song, R.O. Fuentes, R.T. Baker, J. Mater. Chem. 20 (2010) 9760.
[36] R.O. Fuentes, R.T. Baker, Int. J. Hydrogen Energy 33 (2008) 3480.
[37] R.O. Fuentes, R.T. Baker, J. Power Sources 184 (2009) 268.
[38] M.R. Kosinski, R.T. Baker, J. Power Sources 196 (2011) 2498.
[39] R.T. Baker, I.S. Metcalfe, Appl. Catal. A 126 (1995) 297.
[40] F. Duprat, Chem. Eng. Sci. 57 (2002) 901.
[41] H. Vidal, J. Kaspar, M. Pijolat, G. Colon, S. Bernal, A. Cordón, V. Perrichon, F. Fally, Appl. Catal. B 27 (2001) 75.
[42] S. Zhao, R.J. Gorte, Appl. Catal. A 277 (2004) 129.